

# A Neural Rendering Framework for Free-Viewpoint Relighting

Zhang Chen<sup>1</sup>Anpei Chen<sup>1</sup>Guli Zhang<sup>1</sup>Chengyuan Wang<sup>2</sup>Yu Ji<sup>3</sup>Kiriakos N. Kutulakos<sup>4</sup>Jingyi Yu<sup>1</sup><sup>1</sup> ShanghaiTech University<sup>2</sup> Shanghai University<sup>3</sup> DGene, Inc.<sup>4</sup> University of Toronto

{chenzhang, chenap, zhanggl, yujingyi}@shanghaitech.edu.cn ericw385@i.shu.edu.cn

yu.ji@dgene.com

kyros@cs.toronto.edu

## Abstract

We present a novel Relightable Neural Renderer (RNR) for simultaneous view synthesis and relighting using multi-view image inputs. Existing neural rendering (NR) does not explicitly model the physical rendering process and hence has limited capabilities on relighting. RNR instead models image formation in terms of environment lighting, object intrinsic attributes, and the light transport function (LTF), each corresponding to a learnable component. In particular, the incorporation of a physically based rendering process not only enables relighting but also improves the quality of novel view synthesis. Comprehensive experiments on synthetic and real data show that RNR provides a practical and effective solution for conducting free-viewpoint relighting.

## 1. Introduction

Neural rendering (NR) has shown great success in the past few years on producing photorealistic images under complex geometry, surface reflectance, and environment lighting. Unlike traditional modeling and rendering techniques that rely on elaborate setups to capture detailed object geometry and accurate surface reflectance models, often also with excessive artistic manipulations, NR can produce compelling results by using only input images captured under uncontrolled illumination. By far, most existing NR methods have focused on either free-viewpoint rendering under fixed illumination or image-based relighting under fixed viewpoint. In this paper, we explore the problem of simultaneous novel view synthesis and relighting using NR.

State-of-the-art deep view synthesis techniques follow the pipeline that first extract deep features from the input sample images and 3D models, then project the features to the image space via traditional camera projection, and finally apply a rendering network to render the projected features to a RGB image. Such approaches exploit learnable



Figure 1. Results from our Relightable Neural Renderer (RNR). Top row shows the relighting results for a synthetic sphere composed of complex materials. Bottom row shows free-viewpoint relighting results for real captured data.

components to both encode 3D representations and model the rendering process. Approaches such as neural point cloud [2], neural volume [63] and neural texture [69] utilize deep representations for 3D content. With rich training data, these methods can tolerate inaccuracies in geometry and maintain reasonable rendering quality. For example, DeepVoxels [63] proposes to use a learnable volume as an alternative to standard 3D representation while combining physically-based forward/backward projection operators for view synthesis.

Using NR to produce visually plausible free-viewpoint relighting is more difficult compared with changing viewpoints with fixed illumination. This is because under fixed illumination, existing NRs manage to model 2D/3D geometry as learnable components to directly encode appearance of different views. Relighting, in contrast, requires further separating appearance into object intrinsic attributes and illumination. From a NR perspective, the final rendering step in existing approaches cannot yet achieve such separation.

In this paper, we present a novel Relightable Neural Renderer (RNR) for view synthesis and relighting from multi-view inputs. A unique step in our approach is that we model

image formation in terms of environment lighting, object intrinsic attributes, and the light transport function (LTF). RNR sets out to conduct regression on these three individual components rather than directly translating deep features to appearance as in existing NR. In addition, the use of LTF instead of a parametric BRDF model extends the capability of modeling global illumination. While enabling relighting, RNR can also produce view synthesis using the same network architecture. Comprehensive experiments on synthetic and real data show that RNR provides a practical and effective solution for conducting free-viewpoint relighting.

## 2. Related Work

**Image-based Rendering (IBR).** Traditional IBR methods [16, 36, 23, 5, 7, 86, 22, 57] synthesize novel views by blending pixels from input images. Compared with physically based rendering, which requires high-resolution geometry and accurate surface reflectance, they can use much lower quality geometry as proxies to produce relatively high quality rendering. The ultimate rendering quality, however, is a trade-off between the density of the sampling images and geometry: low quality geometry requires dense sampling to reduce visual artifacts; otherwise the rendering exhibits various artifacts including ghosting, aliasing, misalignment and appearance jumps. The same trade-off applies to image-based relighting, although for low frequency lighting, sparse sampling may suffice the need of realistic appearance. Hand-crafted blending schemes [8, 34, 52, 22, 57] have been developed for specific rendering tasks but they generally require extensive parameter tuning.

**Deep View Synthesis.** Recently, there has been a large corpus of works on learning-based novel view synthesis. [68, 12] learn an implicit 3D representation by training on synthetic datasets. Warping-based methods [88, 55, 67, 90, 27, 10] synthesize novel views by predicting the optical flow field. Flow estimation can also be enhanced with geometry priors [87, 44]. Kalantari *et al.* [29] separate the synthesis process into disparity and color estimations for light field data. Srinivasan *et al.* [66] further extend to RGB-D view synthesis on small baseline light fields.

Eslami *et al.* [13] propose Generative Query Network to embed appearances of different views in latent space. Disentangled understanding of scenes can also be conducted through interpretable transformations [82, 35, 77], Lie groups-based latent variables [14] or attention modules [6]. Instead of 2D latent features, [72, 51, 19] utilize volumetric representations as a stronger multi-view constraint whereas Sitzmann *et al.* [64] represents a scene as a continuous mapping from 3D geometry to deep features.

To create more photo-realistic rendering for a wide viewing range, [21, 70, 9, 63, 46, 69, 2, 61, 48, 79] require many

more images as input. Hedman *et al.* [21] learn the blending scheme in IBR. To render view-dependent objects, Thies *et al.* [70] model the view-dependent component with self-supervised learning and then combine it with the diffuse component. Chen *et al.* [9] apply fully connected networks to model the surface light field by exploiting appearance redundancies. Volume-based methods [63, 46] utilize learnable 3D volume to represent scene and combine with projection or ray marching to enforce geometric constraint. Thies *et al.* [69] present a novel learnable neural texture to model rendering as image translation. They use coarse geometry for texture projection and offer flexible content editing. Aliev *et al.* [2] directly use neural point cloud to avoid surface meshing. Auxiliary information such as poses can be used to synthesize more complex objects such as human bodies [61].

To accommodate relighting, Meshry *et al.* [48] learn an embedding for appearance style whereas Xu *et al.* [79] use deep image-based relighting [81] on multi-view multi-light photometric images captured using specialized gantry. Geometry-differentiable neural rendering [58, 45, 43, 39, 31, 47, 84, 42, 26, 71, 50] can potentially handle relighting but our technique focuses on view synthesis and relighting without modifying 3D geometry.

**Free-Viewpoint Relighting.** Earlier free-viewpoint relighting of real world objects requires delicate acquisitions of reflectance [17, 75, 76] while more recent low-cost acquisition approaches still require controlled active illumination or known illumination/geometry [49, 24, 89, 78, 15, 83, 41, 30, 11, 40, 80]. Our work aims to use multi-view images captured under single unknown natural illumination. Previous approaches solve this ill-posed problem via spherical harmonics (SH) [85] or wavelets [18] or both [38] to represent illumination and a parametric BRDF model. Imber *et al.* [25] extract pixel-resolution intrinsic textures. Despite these advances, accurate geometry remains as key component for reliable relighting whereas our RNR aims to simultaneously compensate for geometric inaccuracy and disentangle intrinsic properties from lighting. Tailored illumination models can support outdoor relighting [59, 20, 60] or indoor inverse rendering [3] whereas our RNR uses a more generic lighting model for learning the light transport process. Specifically, our work uses a set of multi-view images of an object under fixed yet unknown natural illumination as input. To carry out view projection and texture mapping, we assume known camera parameters of the input views and known coarse 3D geometry of the object, where standard structure-from-motion and multi-view stereo reconstruction can provide reliable estimations.

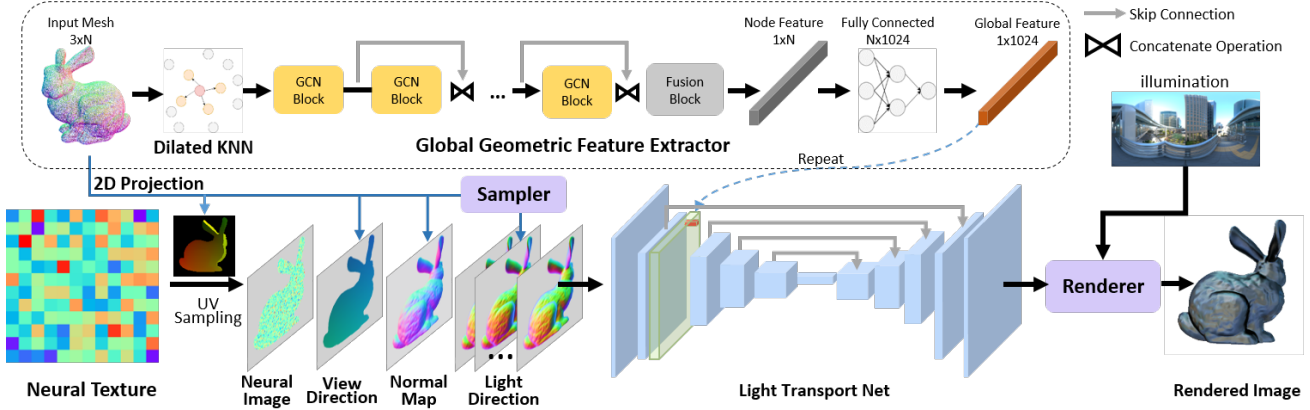


Figure 2. The neural rendering pipeline of RNR.

### 3. Image Formation Model

Under the rendering equation [28], the radiance  $\mathbf{I}$  emitting from point  $\mathbf{x}$  at viewing direction  $\omega_o$  can be computed as:

$$\mathbf{I}(\mathbf{x}, \omega_o) = \int_{S^2} f_r(\mathbf{x}, \omega_i, \omega_o) v(\mathbf{x}, \omega_i) L(\mathbf{x}, \omega_i) \mathbf{n} \cdot \omega_i d\omega_i \quad (1)$$

where  $L(\mathbf{x}, \omega_i)$  is the irradiance that arrives at point  $\mathbf{x}$  from direction  $\omega_i$ . For an environment map, each pixel can be treated as a light source and its intensity is used as irradiance.  $v(\mathbf{x}, \omega_i)$  denotes the visibility of  $\mathbf{x}$  from direction  $\omega_i$  and  $f_r(\mathbf{x}, \omega_i, \omega_o)$  is the bidirectional reflectance distribution function (BRDF) that describes the ratio of outgoing radiance over the incoming irradiance.

Instead of separately conducting regression to recover each individual term in Eq. 1, we learn the light transport function (LTF)  $\mathbf{T}(\mathbf{x}, \omega_i, \omega_o) = f_r(\mathbf{x}, \omega_i, \omega_o) v(\mathbf{x}, \omega_i) \mathbf{n} \cdot \omega_i$ . By separating view-independent albedo from LTF, we have

$$\mathbf{I}(\mathbf{x}) = \int_{S^2} \rho(\mathbf{x}) \mathbf{T}(\mathbf{x}, \omega_i, \omega_o) L(\omega) d\omega \quad (2)$$

The key observation here is that, for static objects, the LTF can be decoupled from illumination. This allows us to decompose photometric attributes into albedo, light transport and illumination for conducting relighting. Specifically, our RNR uses a network to represent the LTF  $\mathbf{T}(\cdot)$ . Learning the LTF instead of the BRDF has several advantages. First, it can compensate for outlier effects such as incorrect visibility caused by inaccurate 3D proxy common in IBR. Second, light transport can represent more complex lighting effects such as inter-reflection. Finally, it reduces the computation when evaluating the radiance of a pixel. It is worth noting that inferring the LTF can be viewed as the inverse problem of precomputed radiance transfer (PRT) [65] which is widely used in physically based rendering.

Same as previous relighting techniques, we assume illumination can be modelled using Spherical Harmonics (SH) up to order 10. The implicit assumption here is that the object cannot be too specular or mirror like. Under the SH representation, Eq. 2 can be written as:

$$\mathbf{I}(\mathbf{x}) = \int_{S^2} \rho(\mathbf{x}) \mathbf{T}(\mathbf{x}, \omega_i, \omega_o) \sum_k c_k Y_k(\omega) d\omega, \quad (3)$$

where  $Y_k$  is the  $k$ th SH basis and  $c_k$  its coefficient. Following common practices, we further decompose the albedo into diffuse albedo  $\rho_d$  and specular albedo  $\rho_s$ .

**Illumination Initialization.** Our SH representation contains 121 coefficients for each color channel. We first exploit the background regions of multi-view images to initialize illumination. We assume that background pixels lie faraway, so we establish the image-to-perspective mapping and fill in the environment map with image pixels. We take the median of the image pixels that map to the same position in environment map to reduce ghosting artifacts. We then project the environment map onto SH basis to obtain the initial value of SH coefficients.

**Neural Texture.** Neural texture [69] provides an efficient encoding of latent properties of 3D scenes. It can be seen as an extension of traditional texture-space data such as color texture, normal map, displacement map, etc. While these data record certain hand-crafted properties of 3D content, neural texture is learnable and can be trained to encode the critical information for a given task (e.g., novel view synthesis). We use the first 3 channels of neural texture as diffuse albedo and second 3 channels as specular albedo. For the rest channels, we leave them unconstrained so as to encode latent properties. To project neural texture to image space, we first rasterize 3D proxy using camera parameters

to obtain uv map (texel-to-pixel mapping) and use bilinear interpolation to sample features from neural texture. Following [69], we use a 4-level mipmap Laplacian pyramid and set the resolution of the top level as  $512 \times 512$ . We also evaluate the first 9 SH coefficients at per-pixel view direction and multiply with channel 7-15 of projected neural texture (neural image).

## 4. Relightable Neural Renderer (RNR)

Next, we set out to simultaneously estimate the albedos  $\rho_d, \rho_s$ , the LTF  $T(\cdot)$  and the SH coefficients  $c_k$ . We use the neural texture [69] to encode the albedo and additional latent properties of the object. We then propose a sampler to sample light directions for evaluating Eq. 2. Next, we propose a Light-Transport-Net (LTN) to predict light transport at the sampled light directions for each pixel. Note that the complete process is differentiable and only require 2D supervision from input multi-view images. Fig.2 shows our pipeline.

### 4.1. Light Direction Sampling

Instead of densely sampling light directions for each vertex (high angular resolution but low spatial resolution), we resort to sparsely sampling light directions for each pixel (low angular resolution but high spatial resolution). In this case, high rendering quality can be achieved even with coarse 3D proxy. We argue that under SH lighting, using sparse light direction sampling only leads to minor inaccuracy on the radiance evaluated in Eq. 3, which can be effectively compensated by LTN.

Since diffuse and specular light transport behaves differently based on light direction and view direction, we utilize different sampling schemes, as shown in Fig.3. For the diffuse component, we first construct  $k_d$  cones centered around the surface normal with half angles of  $\{\theta_1^d, \theta_2^d, \dots, \theta_{k_d}^d\}$ . Then we uniformly sample directions on each cone. This is motivated by the fact that diffuse light transport (ignoring visibility and other effects) follows a cosine attenuation based on the angle between light direction and surface normal. Therefore, light direction nearer to the surface normal are more likely to contribute more to the radiance at that point. For the specular component, we similarly construct  $k_s$  cones around the surface normal and uniformly sample on these cones to obtain halfway directions. Then we reflect view direction around these halfway directions to obtain sampled light directions. This is motivated by the microfacets theory which models surfaces as collections of perfect mirror microfacets. The normals of these microfacets follow a normal distribution function, which we assume to cluster around the macro surface normal. We first carry out light direction sampling in tangent space and then

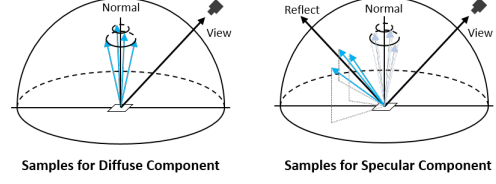


Figure 3. Light direction sampling schemes for diffuse and specular components.

transform to world space by

$$\omega_i(\mathbf{x}) = \mathbf{R}_{TBN}(\mathbf{x}) \cdot \omega'_i(\mathbf{x}), \quad (4)$$

where  $\omega'_i(\mathbf{x})$  is the sampled directions in tangent space and  $\mathbf{R}_{TBN}(\mathbf{x})$  is the rotation matrix from tangent space to world space. By stacking the light directions along the channel dimension, we form a light direction map, which is then input to LTN.

### 4.2. Light Transport Estimation

Our LTN consists of a graph convolutional network (GCN) to extract global geometric features and a modified U-Net to predict per-pixel light transports at sampled light directions.

We first concatenate projected neural texture with view direction map, normal map and light direction map as input to the U-Net. As 2D convolutional network does not fully exploit information in a non-Euclidean structure data, we further augment U-Net with a GCN [33, 4] to extract global features of the 3D geometry. Inspired by [62, 74], we use dynamic edge connections during the training of GCN to learn a better graph representations. But different from [74], which changes the edge connection by finding the nearest neighbour of each vertex, we follow the step of [73, 37] and apply a dilated K-NN method on feature space to search the neighborhood of each vertex. Moreover, rather than using naive GCN, we utilize DenseGCN - a much deeper GCN with residual blocks [37] to gather higher-level features of each vertex. At the end of the DenseGCN, a fully connected layer is applied to fuse all the features into global geometric features. We repeat and concatenate this feature vector with the U-Net feature map after the first downsample layer. This allows light transport estimation to incorporate global geometric information rather than limited to features within a single view.

The output of the U-Net is a light transport map, which contains the light transport at each sampled light direction of each pixel. To render an image, we first retrieve the illumination irradiance on each sampled light direction, and then integrate with albedo and light transport following Eq. 2. Notice that we carry out the integration separately for the diffuse and specular component and then sum these two components to obtain the final image.

### 4.3. Loss Functions

We use  $\ell_1$  loss for the difference between rendered images and ground-truth images:

$$\mathcal{L}_{im} = \frac{1}{n} \sum_{\mathbf{x}} \|\mathbf{I}(\mathbf{x}) - \mathbf{I}_{render}(\mathbf{x})\|_1, \quad (5)$$

where  $n$  is the number of image pixels. However, with  $\ell_1$  loss alone, we cannot guarantee correct relighting. This is due to the ambiguity between albedo, light transport and illumination in Eq. 3: the network can still overfit training images with an incorrect combination of the three components. Therefore, we need to apply additional losses to ensure the network learns a physically plausible interpretation.

**Chromaticity of Light Transport** To constrain the learned light transport function, we propose a novel loss on the chromaticity of light transports. For a pixel, while its light transports at different light directions differ in intensity, they should share similar chromaticity. However, for pixels with low intensities, their light transports may contain a visibility of 0 and hence do not have valid chromaticities. Therefore, we formulate a weighted chromaticity loss on light transport as:

$$\mathcal{L}_{chr} = \frac{1}{nm} \sum_{\mathbf{x}} \sum_{\omega_i} w(\mathbf{x})(1 - \mathbf{T}'(\mathbf{x}, \omega_i, \omega_o) \cdot \mathbf{T}'_{mean}(\mathbf{x}, \omega_o)), \quad (6)$$

where  $m$  is the number of sampled light directions,  $w(\mathbf{x}) = \min(20 \cdot \|\mathbf{I}(\mathbf{x})\|_2, 1)$  is a weight depending on image intensity.  $\mathbf{T}'(\mathbf{x}, \omega_i, \omega_o) = \frac{\mathbf{T}(\mathbf{x}, \omega_i, \omega_o)}{\|\mathbf{T}(\mathbf{x}, \omega_i, \omega_o)\|_2}$  is the chromaticity of a light transport and  $\mathbf{T}'_{mean}(\mathbf{x}, \omega_o)$  is the mean chromaticity for the light transports at pixel  $\mathbf{x}$ .

**Illumination** Although the initial environment map stitched from input multi-view images contains artifacts such as ghosting, the corresponding SH-based environment map is smooth and relatively accurate. Therefore, we would like to constrain our final estimated illumination to be close to the initial one within the regions that are initially covered. We first uniformly sample 4096 directions in the unit sphere and then compute loss based on the SH irradiance on these directions:

$$\mathcal{L}_{illum} = \frac{1}{p} \sum_{\mathbf{p}} \sum_k \|c_k Y_k(\mathbf{p}) - c'_k Y_k(\mathbf{p})\|_1 \quad (7)$$

where  $p$  is the number of directions within initial covered regions,  $c_k$  is estimated SH coefficients and  $c'_k$  is initial SH coefficients.

**Albedo** From Eq. 3, we can see that there is a scale ambiguity between albedo and light transport. Hence, we include a regularization on albedo so that its mean is close to 0.5:

$$\mathcal{L}_{alb} = \frac{1}{q} \sum_{\mathbf{x}} \|\rho(\mathbf{x}) - 0.5\|_1, \quad (8)$$

where  $q$  is the number of texels. This loss is applied to both diffuse and specular albedo.

Our total loss is a weighted composition of the above losses:

$$\mathcal{L} = \mathcal{L}_{im} + \lambda_{chr} \mathcal{L}_{chr} + \lambda_{illum} \mathcal{L}_{illum} + \lambda_{alb} \mathcal{L}_{alb}. \quad (9)$$

## 5. Experimental Results

We implement our method in PyTorch [56]. Before training, we precompute uv map along with the view direction map, normal map and per-pixel tangent space transformation matrix for each training view. We remove the parts in initial 3D proxy that correspond to background. We use a downsampled mesh with 7,500 vertices per model as input to DenseGCN. For neural texture, we use 24 channels. For light direction sampling, we set the half angles of cones to  $\{20^\circ, 40^\circ\}$  for the diffuse component and  $\{5^\circ, 10^\circ\}$  for the specular component. Our experiments reveal that denser sampling only provides marginal improvements. We train our end-to-end network using Adam[32] as the optimizer, with a learning rate of 0.001,  $\beta_1 = 0.9$ ,  $\beta_2 = 0.999$ . We set  $\lambda_{chr} = \lambda_{illum} = \lambda_{alb} = 1$  and train our models for 20k to 50k iterations based on object complexity.

### 5.1. Evaluations on Synthetic Data

We first evaluate RNR on synthetic data for both novel view synthesis and relighting. We choose 4 objects with different geometry complexity, for each we render 200 randomly sampled views under 2 different illuminations. We purposely set the illuminations to have different brightness and color tones. For rendering, we use a physically based renderer - Tungsten [1] to render at a resolution of  $1024 \times 1024$ . We further use different material configurations for each object, ranging from nearly diffuse to moderately specular, and from single material to multiple materials. Example images are shown in the first 4 rows of Fig.4. As aforementioned, our technique cannot handle highly specular objects.

**Novel View Synthesis.** We compare our approach with two state-of-the-art view synthesis methods: DeepVoxels [63] and Deferred Neural Rendering (DeferredNR) [69]. These two methods and ours require per-scene training. For each object, we randomly select 180 images under the first illumination as training views and use the rest 20 for testing. We downsample the images to  $512 \times 512$  before feeding into the three methods and set an equal batch size of 1. At each iteration, DeepVoxels takes one source view and two additional target views as input whereas DeferredNR and ours only require one view as input. For Deepvoxels, we use their implementation and the default hyperparameters. For DeferredNR, we implement our own version since it is not yet open source. We further increase the number

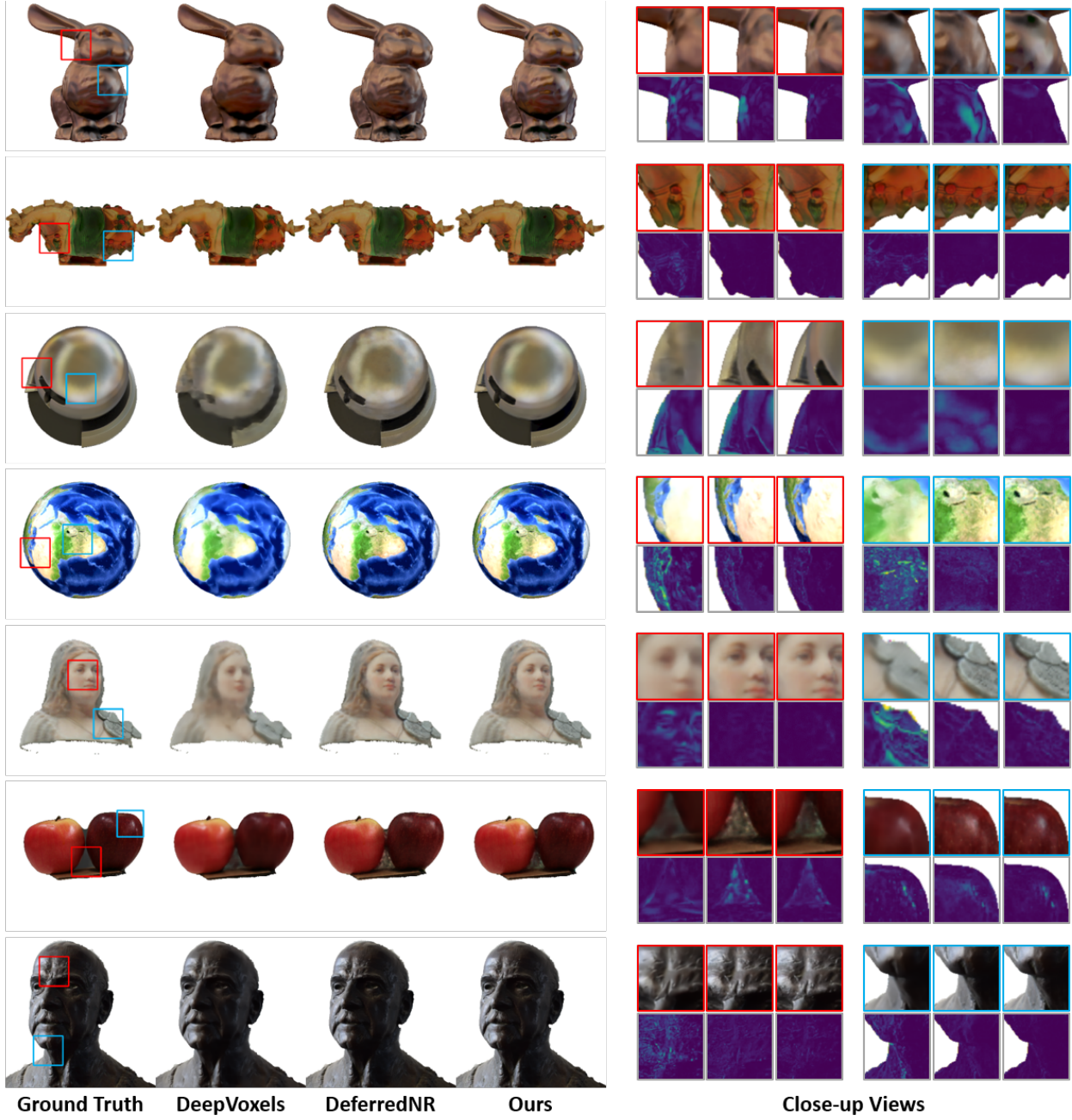


Figure 4. Comparisons on view synthesis. The top 4 rows show the rendered data and bottom 3 show the captured real data. The top row of close-up views shows details on the synthesized views and the second row shows the error maps.

Table 1. Quantitative comparisons of our RNR vs. DeepVoxels [63] and DeferredNR [69] on view synthesis.

Method	Bunny	Horse	Material	Earth	Beauty	Apple	Dyke
DeepVoxels	26.67/0.86	27.98/0.89	28.92/0.93	21.00/0.75	22.05/0.81	19.39/0.75	29.75/0.94
DeferredNR	31.53/0.93	36.44/0.97	30.93/0.93	30.13/0.96	<b>28.12/0.87</b>	26.05/0.89	36.36/ <b>0.98</b>
RNR(Ours)	<b>37.76/0.97</b>	<b>38.33/0.98</b>	<b>34.25/0.96</b>	<b>31.39/0.97</b>	28.05/ <b>0.91</b>	<b>27.81/0.91</b>	<b>36.91/0.98</b>

of neural texture channels as well as the feature channels in

the rendering network to match the number of parameters



Figure 5. Relighting results using RNR on synthetic data. The top row shows the ground truth, the second RNR relighting results, and the bottom the error maps.



Figure 6. Ablation study on losses. On top left shows PSNR and SSIM.

to ours. We notice slight improvements with this modification. Since our goal is to synthesize views of the object instead of the entire scene, we only compute the loss for the pixels on the object for all three methods. For each object, we train our network for an equal or smaller number of iterations than the other two methods. The left 4 columns in Table 1 compare the PSNR and SSIM on the synthetic images. Our proposed method outperforms the two state-of-the-art by a noticeable margin in almost all cases. Qualitative comparisons, close-up views, and error maps are shown in the first 4 rows of Fig.4. Compared to ours, Deepvoxels produces over-smoothed results whereas DeferredNR introduces higher errors near specular highlights, as shown in the 1st and 3rd rows. This illustrates the benefits of encoding the image formation model in rendering process.

**Free-Viewpoint Relighting.** For each object, we use the model trained under the first illumination to carry out free-viewpoint relighting, verified by using the second illumination rendered at a new viewpoint. We compare the synthesized results with the rendered ground truth in Fig.5. Table. 2 shows the evaluation metrics for each object. In addition, we analyze the importance of each loss in Fig.6. Without light transport chromaticity loss or illumination loss, we observe the learnable components will overfit the training data

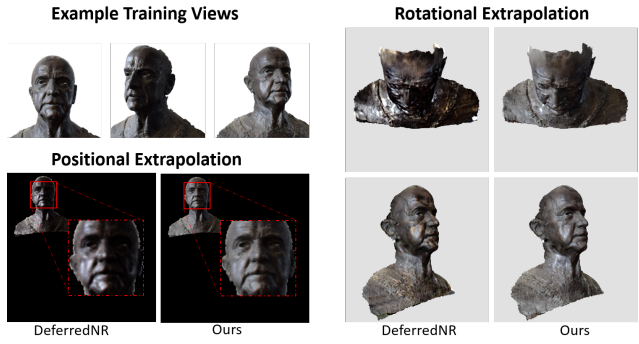


Figure 7. Comparisons of our RNR vs. DeferredNR [69] on view extrapolation.

Table 2. Quantitative evaluations using RNR on relighting synthetic scenes.

Metric	Earth	Bunny	Material	Horse
PSNR	28.66	25.13	25.13	31.11
SSIM	0.95	0.92	0.90	0.94

Table 3. Quantitative comparisons of our RNR vs. DeferredNR [69] on view synthesis using sparse inputs.

Data	DeferredNR	RNR	RNR (Relight)
Bunny	24.38/0.81	<b>30.87/0.94</b>	22.47/0.85
Earth	22.10/0.86	<b>25.32/0.91</b>	25.41/0.90

and lead to incorrect disentangling of the photometric components. This illustrates the importance of our regularization terms.

**Number of Training Views.** To illustrate the effectiveness of RNR in encoding geometric and photometric representations, we further carry out an experiment using sparse input views (20 views in our case). Table. 3 illustrates the PSNR and SSIM measure for view synthesis and relighting. We observe that the performance of DeferredNR degrades drastically when using a small number of training views. In contrast, RNR suffers much less degradation in performance in both tasks. This illustrates the effectiveness in encoding the image formation model. Specifically, compared with a black box solution, RNR can interpret object appearance following the actual physically-based rendering model, thus boosts its generalization to unseen views and lighting.

## 5.2. Evaluations on Real Data

We have also compared RNR with DeepVoxels and DeferredNR on 3 real scenes: Beauty, Apple, Dyck. We captured the first two scenes using a handheld DSLR, with the objects positioned on a tripod. Dyck is directly adopted from DeepVoxels, captured as a video sequence. Beauty and Apple contain 151 and 144 views. For Dyck, we first remove images that contain excessive motion blurs and use

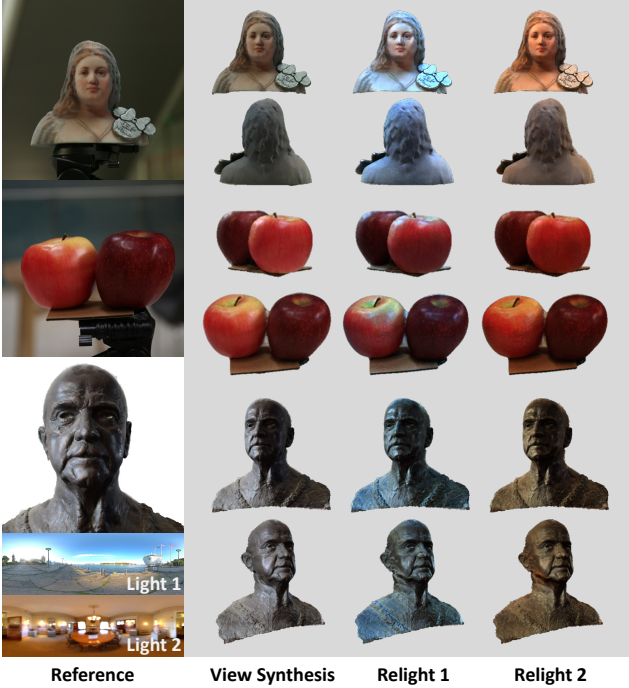


Figure 8. Relighting results on real data.

the remaining 224 views. We use structure-from-motion software Agisoft Photoscan to estimate camera parameters as well as 3D proxy. Similar to synthetic data, we use 90% of the images for training and 10% for testing. The right 3 columns in Table 1 shows the performance of each method, where our method performs the best for most cases. The last 3 rows of Fig.4 show the visual comparisons. DeferredNR produces similar results as RNR although RNR manages to better preserve sharp details in Beauty. Fig.7 shows the view extrapolation results using DeferredNR and RNR. We observe DeferredNR exhibits visual artifacts such as incorrect highlights and color blocks whereas RNR produces more coherent estimations. Please refer to the supplementary video and material for additional results.

We further apply relighting to Beauty, Apple and Dyck in Fig.8. It is worth noting that Dyck only contains views from the front, i.e., the initial illumination stitched by our method only covers a small portion of the entire environment map. Yet RNR manages to produce reasonable relighting results.

To evaluate accuracy in relighting, we use an additional Pig scene from Multi-view Objects Under the Natural Illumination Database [53]. The data contains HDR images captured under 3 different illuminations, each with about 16 calibrated views. We use the views captured in “outdoor” illumination for training. Since the source images are tightly cropped at the object, we are not able to stitch the initial illumination. Hence we use the ground truth illumination in this experiment. The reconstructed geometry in [53] is

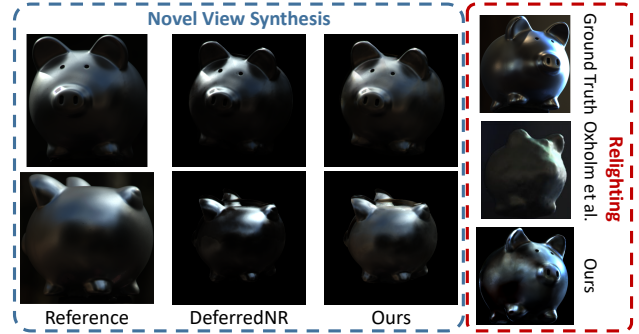


Figure 9. Comparisons on view synthesis and relighting using data from [53].

not publicly available and we use the laser-scanned mesh followed by smoothing and simplification as our 3D proxy.

For testing, we synthesize with the camera parameters and illumination corresponding to a novel view under “indoor” illumination. Fig.9 shows our synthesized result vs. [54] and the ground truth. We observe results produced by RNR appear more realistic than [54], although RNR incurs inaccuracy in highlight and color. This is partially attributed to the low number of training views as well as inaccurate camera parameters provided by the dataset. The left columns in Fig.9 show that our view synthesis is also more reliable than DeferredNR.

## 6. Conclusions and Future Work

We have presented a new neural rendering scheme called Relightable Neural Renderer (RNR) for simultaneous view synthesis and relighting. RNR has exploited the physically based rendering process and separate appearance into environment lighting, object intrinsic attributes, and the light transport function (LT). All three components are learnable through deep networks. In particular, we have shown that by incorporating rendering constraint, our method not only enables relighting but also produces better generalization for novel view synthesis. We have also produced new synthetic and real datasets for both training and validation.

Our current approach cannot yet refine geometry or adaptively sample light directions. When 3D proxy contains severe artifacts, they also negatively impact rendering quality. We refer readers to supplementary material for failure cases. We also do not explicitly handle the lack of dynamic range during data capture, which may influence relighting quality. A possible way is to learn the conversion from low dynamic range image inputs to the HDR ones. In addition, RNR cannot handle highly specular objects and in the future all-frequency lighting representation can be used in conjunction with LT for free-viewpoint relighting of highly specular objects.

## References

- [1] <https://github.com/tunabrain/tungsten>. 5
- [2] Kara-Ali Aliev, Dmitry Ulyanov, and Victor Lempitsky. Neural point-based graphics. *arXiv preprint arXiv:1906.08240*, 2019. 1, 2
- [3] Dejan Azinović, Tzu-Mao Li, Anton Kaplanyan, and Matthias Nießner. Inverse path tracing for joint material and lighting estimation. *arXiv preprint arXiv:1903.07145*, 2019. 2
- [4] Michael M Bronstein, Joan Bruna, Yann LeCun, Arthur Szlam, and Pierre Vandergheynst. Geometric deep learning: going beyond euclidean data. *IEEE Signal Processing Magazine*, 34(4):18–42, 2017. 4
- [5] Chris Buehler, Michael Bosse, Leonard McMillan, Steven Gortler, and Michael Cohen. Unstructured lumigraph rendering. In *Proceedings of the 28th annual conference on Computer graphics and interactive techniques*, pages 425–432. ACM, 2001. 2
- [6] Christopher P Burgess, Loic Matthey, Nicholas Watters, Rishabh Kabra, Irina Higgins, Matt Botvinick, and Alexander Lerchner. Monet: Unsupervised scene decomposition and representation. *arXiv preprint arXiv:1901.11390*, 2019. 2
- [7] Joel Carranza, Christian Theobalt, Marcus A Magnor, and Hans-Peter Seidel. *Free-viewpoint video of human actors*, volume 22. ACM, 2003. 2
- [8] Gaurav Chaurasia, Sylvain Duchene, Olga Sorkine-Hornung, and George Drettakis. Depth synthesis and local warps for plausible image-based navigation. *ACM Transactions on Graphics (TOG)*, 32(3):30, 2013. 2
- [9] Anpei Chen, Minye Wu, Yingliang Zhang, Nianyi Li, Jie Lu, Shenghua Gao, and Jingyi Yu. Deep surface light fields. *Proceedings of the ACM on Computer Graphics and Interactive Techniques*, 1(1):14, 2018. 2
- [10] Xu Chen, Jie Song, and Otmar Hilliges. Nvs machines: Learning novel view synthesis with fine-grained view control. *arXiv preprint arXiv:1901.01880*, 2019. 2
- [11] Valentin Deschaintre, Miika Aittala, Fredo Durand, George Drettakis, and Adrien Bousseau. Single-image svbrdf capture with a rendering-aware deep network. *ACM Transactions on Graphics (TOG)*, 37(4):128, 2018. 2
- [12] Alexey Dosovitskiy, Jost Tobias Springenberg, Maxim Tatarchenko, and Thomas Brox. Learning to generate chairs, tables and cars with convolutional networks. *IEEE transactions on pattern analysis and machine intelligence*, 39(4):692–705, 2016. 2
- [13] SM Ali Eslami, Danilo Jimenez Rezende, Frederic Besse, Fabio Viola, Ari S Morcos, Marta Garnelo, Avraham Ruderman, Andrei A Rusu, Ivo Danihelka, Karol Gregor, et al. Neural scene representation and rendering. *Science*, 360(6394):1204–1210, 2018. 2
- [14] Luca Falorsi, Pim de Haan, Tim R Davidson, Nicola De Cao, Maurice Weiler, Patrick Forré, and Taco S Cohen. Explorations in homeomorphic variational auto-encoding. *arXiv preprint arXiv:1807.04689*, 2018. 2
- [15] Duan Gao, Xiao Li, Yue Dong, Pieter Peers, Kun Xu, and Xin Tong. Deep inverse rendering for high-resolution svbrdf estimation from an arbitrary number of images. *ACM Transactions on Graphics (TOG)*, 38(4):134, 2019. 2
- [16] Steven J Gortler, Radek Grzeszczuk, Richard Szeliski, and Michael F Cohen. The lumigraph. In *Siggraph*, volume 96, pages 43–54, 1996. 2
- [17] Darya Guarnera, Giuseppe Claudio Guarnera, Abhijeet Ghosh, Cornelia Denk, and Mashhuda Glencross. Brdf representation and acquisition. In *Computer Graphics Forum*, volume 35, pages 625–650. Wiley Online Library, 2016. 2
- [18] Tom Haber, Christian Fuchs, Philippe Bekaer, Hans-Peter Seidel, Michael Goesele, and Hendrik PA Lensch. Relighting objects from image collections. In *2009 IEEE Conference on Computer Vision and Pattern Recognition*, pages 627–634. IEEE, 2009. 2
- [19] Adam W Harley, Fangyu Li, Shrividhi K Lakshminikanth, Xian Zhou, Hsiao-Yu Fish Tung, and Katerina Fragkiadaki. Embodied view-contrastive 3d feature learning. *arXiv preprint arXiv:1906.03764*, 2019. 2
- [20] Daniel Cabrini Hauagge, Scott Wehrwein, Paul Upchurch, Kavita Bala, and Noah Snavely. Reasoning about photo collections using models of outdoor illumination. In *BMVC*, 2014. 2
- [21] Peter Hedman, Julien Philip, True Price, Jan-Michael Frahm, George Drettakis, and Gabriel Brostow. Deep blending for free-viewpoint image-based rendering. In *SIGGRAPH Asia 2018 Technical Papers*, page 257. ACM, 2018. 2
- [22] Peter Hedman, Tobias Ritschel, George Drettakis, and Gabriel Brostow. Scalable inside-out image-based rendering. *ACM Transactions on Graphics (TOG)*, 35(6):231, 2016. 2
- [23] Benno Heigl, Reinhard Koch, Marc Pollefeys, Joachim Denzler, and Luc Van Gool. Plenoptic modeling and rendering from image sequences taken by a hand-held camera. In *Mustererkennung 1999*, pages 94–101. Springer, 1999. 2
- [24] Zhuo Hui, Kalyan Sunkavalli, Joon-Young Lee, Sunil Hadap, Jian Wang, and Aswin C Sankaranarayanan. Reflectance capture using univariate sampling of brdfs. In *Proceedings of the IEEE International Conference on Computer Vision*, pages 5362–5370, 2017. 2
- [25] James Imber, Jean-Yves Guillemaut, and Adrian Hilton. Intrinsic textures for relightable free-viewpoint video. In *European Conference on Computer Vision*, pages 392–407. Springer, 2014. 2
- [26] Eldar Insafutdinov and Alexey Dosovitskiy. Unsupervised learning of shape and pose with differentiable point clouds. In *Advances in Neural Information Processing Systems*, pages 2802–2812, 2018. 2
- [27] Shi Jin, Ruiyinag Liu, Yu Ji, Jinwei Ye, and Jingyi Yu. Learning to dodge a bullet: Conyclic view morphing via deep learning. In *Proceedings of the European Conference on Computer Vision (ECCV)*, pages 218–233, 2018. 2
- [28] James T Kajiya. The rendering equation. In *ACM Siggraph Computer Graphics*, volume 20, pages 143–150. ACM, 1986. 3
- [29] Nima Khademi Kalantari, Ting-Chun Wang, and Ravi Ramamoorthi. Learning-based view synthesis for light field cameras. *ACM Transactions on Graphics (TOG)*, 35(6):193, 2016. 2

- [30] Kaizhang Kang, Zimin Chen, Jiaping Wang, Kun Zhou, and Hongzhi Wu. Efficient reflectance capture using an autoencoder. *ACM Trans. Graph.*, 37(4):127–1, 2018. 2
- [31] Hiroharu Kato, Yoshitaka Ushiku, and Tatsuya Harada. Neural 3d mesh renderer. In *Proceedings of the IEEE Conference on Computer Vision and Pattern Recognition*, pages 3907–3916, 2018. 2
- [32] Diederik P Kingma and Jimmy Ba. Adam: A method for stochastic optimization. *arXiv preprint arXiv:1412.6980*, 2014. 5
- [33] Thomas N Kipf and Max Welling. Semi-supervised classification with graph convolutional networks. *arXiv preprint arXiv:1609.02907*, 2016. 4
- [34] Johannes Kopf, Michael F Cohen, and Richard Szeliski. First-person hyper-lapse videos. *ACM Transactions on Graphics (TOG)*, 33(4):78, 2014. 2
- [35] Tejas D Kulkarni, William F Whitney, Pushmeet Kohli, and Josh Tenenbaum. Deep convolutional inverse graphics network. In *Advances in neural information processing systems*, pages 2539–2547, 2015. 2
- [36] Marc Levoy and Pat Hanrahan. Light field rendering. In *Proceedings of the 23rd annual conference on Computer graphics and interactive techniques*, pages 31–42. ACM, 1996. 2
- [37] Guohao Li, Matthias Muller, Ali Thabet, and Bernard Ghanem. Deepgencs: Can gcns go as deep as cnns? In *Proceedings of the IEEE International Conference on Computer Vision*, pages 9267–9276, 2019. 4
- [38] Guannan Li, Chenglei Wu, Carsten Stoll, Yebin Liu, Kiran Varanasi, Qionghai Dai, and Christian Theobalt. Capturing relightable human performances under general uncontrolled illumination. In *Computer Graphics Forum*, volume 32, pages 275–284. Wiley Online Library, 2013. 2
- [39] Tzu-Mao Li, Miika Aittala, Frédéric Durand, and Jaakko Lehtinen. Differentiable monte carlo ray tracing through edge sampling. In *SIGGRAPH Asia 2018 Technical Papers*, page 222. ACM, 2018. 2
- [40] Xiao Li, Yue Dong, Pieter Peers, and Xin Tong. Modeling surface appearance from a single photograph using self-augmented convolutional neural networks. *ACM Transactions on Graphics (TOG)*, 36(4):45, 2017. 2
- [41] Zhengqin Li, Kalyan Sunkavalli, and Manmohan Chandraker. Materials for masses: Svbrdf acquisition with a single mobile phone image. In *Proceedings of the European Conference on Computer Vision (ECCV)*, pages 72–87, 2018. 2
- [42] Chen-Hsuan Lin, Chen Kong, and Simon Lucey. Learning efficient point cloud generation for dense 3d object reconstruction. In *Thirty-Second AAAI Conference on Artificial Intelligence*, 2018. 2
- [43] Hsueh-Ti Derek Liu, Michael Tao, and Alec Jacobson. Paparazzi: surface editing by way of multi-view image processing. *ACM Trans. Graph.*, 37(6):221–1, 2018. 2
- [44] Miaoqiao Liu, Xuming He, and Mathieu Salzmann. Geometry-aware deep network for single-image novel view synthesis. In *Proceedings of the IEEE Conference on Computer Vision and Pattern Recognition*, pages 4616–4624, 2018. 2
- [45] Shichen Liu, Tianye Li, Weikai Chen, and Hao Li. Soft rasterizer: A differentiable renderer for image-based 3d reasoning. *arXiv preprint arXiv:1904.01786*, 2019. 2
- [46] Stephen Lombardi, Tomas Simon, Jason Saragih, Gabriel Schwartz, Andreas Lehrmann, and Yaser Sheikh. Neural volumes: Learning dynamic renderable volumes from images. *arXiv preprint arXiv:1906.07751*, 2019. 2
- [47] Matthew M Loper and Michael J Black. OpenDR: An approximate differentiable renderer. In *European Conference on Computer Vision*, pages 154–169. Springer, 2014. 2
- [48] Moustafa Meshry, Dan B Goldman, Sameh Khamis, Hugues Hoppe, Rohit Pandey, Noah Snavely, and Ricardo Martin-Brualla. Neural rerendering in the wild. In *Proceedings of the IEEE Conference on Computer Vision and Pattern Recognition*, pages 6878–6887, 2019. 2
- [49] Giljoo Nam, Joo Ho Lee, Diego Gutierrez, and Min H Kim. Practical svbrdf acquisition of 3d objects with unstructured flash photography. In *SIGGRAPH Asia 2018 Technical Papers*, page 267. ACM, 2018. 2
- [50] Thu H Nguyen-Phuoc, Chuan Li, Stephen Balaban, and Yongliang Yang. Rendernet: A deep convolutional network for differentiable rendering from 3d shapes. In *Advances in Neural Information Processing Systems*, pages 7891–7901, 2018. 2
- [51] Kyle Olszewski, Sergey Tulyakov, Oliver Woodford, Hao Li, and Linjie Luo. Transformable bottleneck networks. *arXiv preprint arXiv:1904.06458*, 2019. 2
- [52] Rodrigo Ortiz-Cayon, Abdelaziz Djelouah, and George Drettakis. A bayesian approach for selective image-based rendering using superpixels. 2015. 2
- [53] Geoffrey Oxholm and Ko Nishino. Multiview shape and reflectance from natural illumination. In *Proceedings of the IEEE Conference on Computer Vision and Pattern Recognition*, pages 2155–2162, 2014. 8
- [54] Geoffrey Oxholm and Ko Nishino. Shape and reflectance estimation in the wild. *IEEE transactions on pattern analysis and machine intelligence*, 38(2):376–389, 2015. 8
- [55] Eunbyung Park, Jimei Yang, Ersin Yumer, Duygu Ceylan, and Alexander C Berg. Transformation-grounded image generation network for novel 3d view synthesis. In *Proceedings of the ieee conference on computer vision and pattern recognition*, pages 3500–3509, 2017. 2
- [56] Adam Paszke, Sam Gross, Soumith Chintala, Gregory Chanan, Edward Yang, Zachary DeVito, Zeming Lin, Alban Desmaison, Luca Antiga, and Adam Lerer. Automatic differentiation in pytorch. 2017. 5
- [57] Eric Penner and Li Zhang. Soft 3d reconstruction for view synthesis. *ACM Transactions on Graphics (TOG)*, 36(6):235, 2017. 2
- [58] Felix Petersen, Amit H Bermano, Oliver Deussen, and Daniel Cohen-Or. Pix2vex: Image-to-geometry reconstruction using a smooth differentiable renderer. *arXiv preprint arXiv:1903.11149*, 2019. 2
- [59] Julien Philip, Michaël Gharbi, Tinghui Zhou, Alexei A Efros, and George Drettakis. Multi-view relighting using a geometry-aware network. *ACM Transactions on Graphics (TOG)*, 38(4):78, 2019. 2

- [60] Qi Shan, Riley Adams, Brian Curless, Yasutaka Furukawa, and Steven M Seitz. The visual turing test for scene reconstruction. In *2013 International Conference on 3D Vision-3DV 2013*, pages 25–32. IEEE, 2013. [2](#)
- [61] Aliaksandra Shysheya, Egor Zakharov, Kara-Ali Aliev, Renat Bashirov, Egor Burkov, Karim Iskakov, Aleksei Ivakhnenko, Yury Malkov, Igor Pasechnik, Dmitry Ulyanov, et al. Textured neural avatars. In *Proceedings of the IEEE Conference on Computer Vision and Pattern Recognition*, pages 2387–2397, 2019. [2](#)
- [62] Martin Simonovsky and Nikos Komodakis. Dynamic edge-conditioned filters in convolutional neural networks on graphs. In *Proceedings of the IEEE conference on computer vision and pattern recognition*, pages 3693–3702, 2017. [4](#)
- [63] Vincent Sitzmann, Justus Thies, Felix Heide, Matthias Nießner, Gordon Wetzstein, and Michael Zollhofer. Deepvoxels: Learning persistent 3d feature embeddings. In *Proceedings of the IEEE Conference on Computer Vision and Pattern Recognition*, pages 2437–2446, 2019. [1, 2, 5, 6](#)
- [64] Vincent Sitzmann, Michael Zollhöfer, and Gordon Wetzstein. Scene representation networks: Continuous 3d-structure-aware neural scene representations. *arXiv preprint arXiv:1906.01618*, 2019. [2](#)
- [65] Peter-Pike Sloan, Jan Kautz, and John Snyder. Precomputed radiance transfer for real-time rendering in dynamic, low-frequency lighting environments. In *ACM Transactions on Graphics (TOG)*, volume 21, pages 527–536. ACM, 2002. [3](#)
- [66] Pratul P Srinivasan, Tongzhou Wang, Ashwin Sreelal, Ravi Ramamoorthi, and Ren Ng. Learning to synthesize a 4d rgbd light field from a single image. In *Proceedings of the IEEE International Conference on Computer Vision*, pages 2243–2251, 2017. [2](#)
- [67] Shao-Hua Sun, Minyoung Huh, Yuan-Hong Liao, Ning Zhang, and Joseph J Lim. Multi-view to novel view: Synthesizing novel views with self-learned confidence. In *Proceedings of the European Conference on Computer Vision (ECCV)*, pages 155–171, 2018. [2](#)
- [68] Maxim Tatarchenko, Alexey Dosovitskiy, and Thomas Brox. Single-view to multi-view: Reconstructing unseen views with a convolutional network. *arXiv preprint arXiv:1511.06702*, 6, 2015. [2](#)
- [69] Justus Thies, Michael Zollhöfer, and Matthias Nießner. Deferred neural rendering: Image synthesis using neural textures. *arXiv preprint arXiv:1904.12356*, 2019. [1, 2, 3, 4, 5, 6, 7](#)
- [70] Justus Thies, Michael Zollhöfer, Christian Theobalt, Marc Stamminger, and Matthias Nießner. Ignor: Image-guided neural object rendering. *arXiv preprint arXiv:1811.10720*, 2018. [2](#)
- [71] Shubham Tulsiani, Tinghui Zhou, Alexei A Efros, and Jitendra Malik. Multi-view supervision for single-view reconstruction via differentiable ray consistency. In *Proceedings of the IEEE conference on computer vision and pattern recognition*, pages 2626–2634, 2017. [2](#)
- [72] Hsiao-Yu Fish Tung, Ricsen Cheng, and Katerina Fragkiadaki. Learning spatial common sense with geometry-aware recurrent networks. In *Proceedings of the IEEE Conference on Computer Vision and Pattern Recognition*, pages 2595–2603, 2019. [2](#)
- [73] Diego Valsesia, Giulia Fracastoro, and Enrico Magli. Learning localized generative models for 3d point clouds via graph convolution. 2018. [4](#)
- [74] Yue Wang, Yongbin Sun, Ziwei Liu, Sanjay E Sarma, Michael M Bronstein, and Justin M Solomon. Dynamic graph cnn for learning on point clouds. *ACM Transactions on Graphics (TOG)*, 38(5):146, 2019. [4](#)
- [75] Michael Weinmann and Reinhard Klein. Advances in geometry and reflectance acquisition (course notes). In *SIGGRAPH Asia 2015 Courses*, page 1. ACM, 2015. [2](#)
- [76] Tim Weyrich, Jason Lawrence, Hendrik PA Lensch, Szymon Rusinkiewicz, Todd Zickler, et al. Principles of appearance acquisition and representation. *Foundations and Trends® in Computer Graphics and Vision*, 4(2):75–191, 2009. [2](#)
- [77] Daniel E Worrall, Stephan J Garbin, Daniyar Turmukhametov, and Gabriel J Brostow. Interpretable transformations with encoder-decoder networks. In *Proceedings of the IEEE International Conference on Computer Vision*, pages 5726–5735, 2017. [2](#)
- [78] Rui Xia, Yue Dong, Pieter Peers, and Xin Tong. Recovering shape and spatially-varying surface reflectance under unknown illumination. *ACM Transactions on Graphics (TOG)*, 35(6):187, 2016. [2](#)
- [79] Zexiang Xu, Sai Bi, Kalyan Sunkavalli, Sunil Hadap, Hao Su, and Ravi Ramamoorthi. Deep view synthesis from sparse photometric images. *ACM Transactions on Graphics (TOG)*, 38(4):76, 2019. [2](#)
- [80] Zexiang Xu, Jannik Boll Nielsen, Jiyang Yu, Henrik Wann Jensen, and Ravi Ramamoorthi. Minimal brdf sampling for two-shot near-field reflectance acquisition. *ACM Transactions on Graphics (TOG)*, 35(6):188, 2016. [2](#)
- [81] Zexiang Xu, Kalyan Sunkavalli, Sunil Hadap, and Ravi Ramamoorthi. Deep image-based relighting from optimal sparse samples. *ACM Transactions on Graphics (TOG)*, 37(4):126, 2018. [2](#)
- [82] Jimei Yang, Scott E Reed, Ming-Hsuan Yang, and Honglak Lee. Weakly-supervised disentangling with recurrent transformations for 3d view synthesis. In *Advances in Neural Information Processing Systems*, pages 1099–1107, 2015. [2](#)
- [83] Wenjie Ye, Xiao Li, Yue Dong, Pieter Peers, and Xin Tong. Single image surface appearance modeling with self-augmented cnns and inexact supervision. In *Computer Graphics Forum*, volume 37, pages 201–211. Wiley Online Library, 2018. [2](#)
- [84] Wang Yifan, Felice Serena, Shihao Wu, Cengiz Öztireli, and Olga Sorkine-Hornung. Differentiable surface splatting for point-based geometry processing. *arXiv preprint arXiv:1906.04173*, 2019. [2](#)
- [85] Tianli Yu, Hongcheng Wang, Narendra Ahuja, and Wei-Chao Chen. Sparse lumigraph relighting by illumination and reflectance estimation from multi-view images. In *ACM SIGGRAPH 2006 Sketches*, page 175. ACM, 2006. [2](#)
- [86] Ke Colin Zheng, Alex Colburn, Aseem Agarwala, Maneesh Agrawala, David Salesin, Brian Curless, and Michael F Cohen. Parallax photography: creating 3d cinematic effects

- from stills. In *Proceedings of Graphics Interface 2009*, pages 111–118. Canadian Information Processing Society, 2009. 2
- [87] Tinghui Zhou, Richard Tucker, John Flynn, Graham Fyffe, and Noah Snavely. Stereo magnification: Learning view synthesis using multiplane images. *arXiv preprint arXiv:1805.09817*, 2018. 2
- [88] Tinghui Zhou, Shubham Tulsiani, Weilun Sun, Jitendra Malik, and Alexei A Efros. View synthesis by appearance flow. In *European conference on computer vision*, pages 286–301. Springer, 2016. 2
- [89] Zhiming Zhou, Guojun Chen, Yue Dong, David Wipf, Yong Yu, John Snyder, and Xin Tong. Sparse-as-possible svbrdf acquisition. *ACM Transactions on Graphics (TOG)*, 35(6):189, 2016. 2
- [90] Hao Zhu, Hao Su, Peng Wang, Xun Cao, and Ruigang Yang. View extrapolation of human body from a single image. In *Proceedings of the IEEE Conference on Computer Vision and Pattern Recognition*, pages 4450–4459, 2018. 2